applied sciences

MDPI

Article

Predictive Control for Current Distortion Mitigation in Mining Power Grids

Juan S. Gómez [1], Alex Navas-Fonseca [1], Freddy Flores-Bahamonde [1], Luca Tarisciotti [1,*], Cristian Garcia [2], Felipe Nuñez [3], Jose Rodriguez [4] and Aldo Z. Cipriano [3]

[1] Energy Transformation Center, Engineering Faculty, Universidad Andres Bello, Santiago 7500971, Chile
[2] Department of Electrical Engineering, Universidad de Talca, Curico 3340000, Chile
[3] Department of Electrical Engineering, Pontificia Universidad Católica de Chile, Santiago 7820436, Chile
[4] Department of Engineering, Universidad San Sebastián, Santiago 8420524, Chile
* Correspondence: luca.tarisciotti@unab.cl; Tel.: +56-951-391-997

Abstract: Current distortion is a critical issue of power quality because the low frequency harmonics injected by adjustable speed drives increase heating losses in transmission lines and induce torque flickering in induction motors, which are widely used in mining facilities. Although classical active filtering techniques mitigate the oscillatory components of imaginary power, they may not be sufficient to clean the sensitive nodes of undesirable power components, some of which are related to real power. However, the usage of power electronic converters for distributed generation and energy storage, allows the integration of complementary power quality control objectives in electrical systems, by using the same facilities required for active power transferring. This paper proposes a predictive control-based scheme for mitigating the current distortion in the coupling node between utility grid and the mining facility power system. Instead of the classical approach of active filtering, this task is included as a secondary level objective control referred into the microgrid control hierarchy. Hardware-in-the-Loop simulation results showed that the proposed scheme is capable of bounding the current distortion, according to IEEE standard 1547, for both individual harmonics and the total rated current distortion, through inequality constraints of the optimization problem.

Keywords: model predictive control; harmonic current distortion; distributed generation; microgrid; point of common coupling

Citation: Gómez, J.S.; Navas-Fonseca, A.; Flores-Bahamonde, F.; Tarisciotti, L.; Garcia, C.; Nuñez, F.; Rodriguez, J.; Cipriano, A.Z. Predictive Control for Current Distortion Mitigation in Mining Power Grids. *Appl. Sci.* **2023**, *13*, 3523. https://doi.org/10.3390/app13063523

Academic Editors: Levon Gevorkov and Olena Rubanenko

Received: 30 January 2023
Revised: 7 March 2023
Accepted: 7 March 2023
Published: 9 March 2023

1. Introduction

Mining is a critical industry for energy transition because, although it has a considerable environmental footprint, it provides raw materials, such as gold and copper, which are required for electronic devices, transmission lines and electrical machines [1]. Nowadays, the transition of the mining industry towards smarter and cleaner operations includes environment-friendly practices and policies, pursuing an optimal consumption of water and energy, reduction of carbon emissions, and more precise extraction techniques [2]. In this sense, the coexistence of older machinery, such as cycloconverter-based drives in crushers and mills, and newer technologies, such as electrical hauling trucks, is unavoidable during this transition process.

In mining facilities, adjustable frequency drives have been used throughout the whole mining process. Historically, cycloconverter topology was a well-accepted solution for low-speed grinding mills control; however, its related harmonics issues in mining power systems are significant [3]. In this sense, the academic community is currently exploring converters based on multilevel topologies in addition to diode-based rectifiers and active front end (AFE) converters. These converters have been used for high-power mills [4], for medium-power conveyor belts [5,6] and for hauling trucks [7,8]. In contrast to the academic trend, mining companies' transition towards new technologies is slower because additional business concerns must be considered. Therefore, the coexistence of old and new technologies in mining facilities implies a tough challenge to be overcome in the short term.

Although AFE has shown better control capabilities and efficiency than cycloconverters, both of them impact the power quality of the mining power system. For example, cycloconverters inject harmonic distortion to the grid because of the absence of a DC-link or other reactive components that operate as a filter between the machine-side and the grid-side [9]. On the other hand, DC-link and LC-filters of AFE topologies easily reduce high-frequency components, but low-frequency harmonics, below 200 Hz, caused by unbalances, PLLs tracking errors, and nonlinear loads, are reflected in the power system [10].

As a consequence of this low-order harmonics pollution, magnetic flux inside of transformers and motors of mining machinery is affected, and, thus, the damage risks increase [11]. In addition, because of changes in mining facilities over time, long cables and poor design and selection of transformers, the active power transference capacity of the power grid is also reduced. Therefore, mining companies should be aware that power quality improvement at the point of common coupling (PCC) with the utility grid, and other sensitive nodes, represent a more efficient operation of the power system.

The IEEE std 1547 [12] states that the reference points into power systems are those where characteristics, such as voltage, frequency, total rated current distortion, and response-to-failure capabilities, meet the standard. Although PCCs are defined as reference points, it is possible to define additional ones to satisfy internal requirements in the microgrid or power system area. For instance, in the mining industry, electric rope shovels used for ore extraction are sensitive to harmonics pollution and voltage sags/swells. In this case, filtering devices are used to reduce the risk of damage and preserve their operational integrity; however, considering that this type of machinery is replaced according to mine expansion, passive filtering is not an optimal solution [13].

There are two main approaches for managing harmonic distortion issues. The first one considers this issue by directly improving control and modulation algorithms over the power converter. In [14], common mode voltage is mitigated by integrating this objective in a primary controller which states the switching pattern, modifying the classical space vector modulation scheme. The authors of [15] proposed an MPC for hybrid AC/DC microgrids that finds a balance between the power quality and efficiency of the system in order to control the power exchange between the microgrids. In [16], the authors proposed a dual PWM technique to reduce the grid flickering and aliasing distortion caused by low-frequency oscillations that emerge in the power grid when torque disturbances occur in adjustable frequency drives. Model predictive control (MPC) was also used in this approach [17–20]. In [17,18], finite control set MPC applications were reported considering power quality objectives, by minimizing unbalanced and harmonics components, respectively. In [17], unbalances compensation is made through the computation of positive and negative sequences of active and reactive powers, whereas the harmonics detection strategy in [18] uses synchronous reference frames rotating at harmonics frequencies. The authors of [19] proposed an MPC that maintains low current distortion, which is based on dividing the operating regions of the space vector diagram and compensating for absent vectors. Similarly, reference [20] proposed a multi-vector MPC to reduce the current distortion, where the volt–second balance is achieved when three optimal vectors are adopted to synthesize the desired voltage. In these approaches, model predictions are one step ahead and the cost function is computed for each switch's combination.

The second approach states the integration of passive and active filters along the microgrid or power system area, usually close to sensitive nodes; however, it implies the integration of additional hardware. A deep analysis of the selection and design of passive filters for high-power applications in mining is presented in [10]. The authors conclude that C-type filters, and second-order high-pass filters could be used appropriately in mining applications because of their low-order current harmonics attenuation and reactive power compensation properties. On the other hand, active filtering is a widely used technique in the industry to compensate for the pollution caused by unbalances and harmonics. This technique is based on measuring power components from the load to supply and compensating the undesired ones, reducing higher order harmonics at the PCC. The most common frameworks used to state the value of the compensation components are selective harmonics compensation, instantaneous power theory [21], and conservative power theory [22].

Applications of active filtering using instantaneous power and conservative power (CPT) theories have been reported in [23,24], respectively. A remarkable advantage of these techniques is the decomposition of power in direct and oscillatory components, where the latter is controlled to a zero reference; thus, simple controllers, such as proportional integral (PI) controllers, can be used. However, a drawback of such techniques is the low bandwidth of PI controllers, which may not meet the high bandwidth required for controlling the oscillatory components. In this sense, this solution is classified into the primary control level in microgrids or power systems. In contrast, the selection of harmonics to compensate them by injecting a counter-phase current increases the computational burden required for total distortion mitigation but improves the system frequency response. In [25], sliding discrete Fourier transform allows distortion mitigation, by proportional control of each voltage harmonic, as a complementary objective in the primary level of distributed generators. In [26], a set of second-order band-pass filters are defined for harmonics filtering in the $\alpha\beta$ domain, and then compensation components are computed at the primary level as well. Conversely, approaches based on consensus theory to share imbalances [27] and harmonic distortion [28] have been reported. For instance, in reference [27] three-phase MGs are controlled as three single-phase subsystems, where droop reactive power–voltage controllers are employed to share imbalances. The authors of [28] use the CPT to share imbalances and harmonics in four-wires droop-based MGs. The CPT is used to decompose currents and powers in the balanced, unbalanced and distorted components. Then, virtual impedance loops are implemented. Similar approaches for imbalance sharing are proposed in [29–31]. Nevertheless, these approaches are based on PI controllers and use virtual impedance loops computed via power theories. It has been validated that virtual impedance loops do not guarantee the sharing of single-phase powers.

In [32], current harmonics components are detected by using fast Fourier transform and used as initial conditions for a discrete-time model of the converter's output filter. In this case, a continuous control set MPC is used for minimizing the overall system distortion in a marine vessel power grid, and, thus, Kirchhoff laws are used to solve the power flow. By using current as the optimization variable, capacity constraints are included to avoid overpassing maximum values, notably present in the presented simulation results. Another application of continuous control set MPC for power quality is shown in [33], where independent synchronous reference frames are used to estimate phase voltage vectors in order to compensate imbalances in a microgrid. This approach uses consensus of reactive power, among distributed generators, to satisfy phase voltage unbalance rate constraints in a cooperative way.

Based on this context, this paper proposes a novel MPC scheme for current distortion mitigation by including power harmonics compensation and total current distortion as optimization constraints. This MPC-based solution is justified because of the optimal distribution of the control effort along the prediction horizon, and the bounding of the solution space through equality and inequality constraints. The contributions of this work are stated as follow:

- A frequency harmonics decomposition of real power is proposed, enabling control of their magnitudes by an MPC and of their angle phases by a traditional PI controller.
- A reformulation of the MPC optimization problem is performed, in order to control two current harmonics components by manipulating one power harmonic component and satisfying current distortion requirements imposed by IEEE std 1547.
- As a result of previous contributions, the proposed scheme was validated in a Hardware-In-the-Loop (HIL) system, validating its capability to be synthesized in real-time applications and embedded devices.

The rest of this paper is organized as follows. In Section 2 preliminary concepts and the mathematical formulation of power bounds to current harmonics control are derived. In Section 3, the optimization problem used by the MPC scheme is stated, whereas a real-time simulation setup and the results of this proposal are presented in Section 4. Finally, conclusions are drawn in Section 5.

2. Preliminaries

In this section, preliminary background about instantaneous power is provided. The assumptions and mathematical derivation of power boundaries required for current harmonics control are also presented. Furthermore, Figure 1 presents the equivalent model used in this work, where the load Z_1 demands harmonics components to be supplied by the power system. Therefore, to optimize the power flow through the PCC, only the fundamental component, and, thus, active power is transferred and the control scheme of the Distributed Generator (DG) should supply harmonics components. The following subsections analyze the real power transferred from the PCC to the load, in order to synthesize the DG controller. The latter is presented in Section 3.

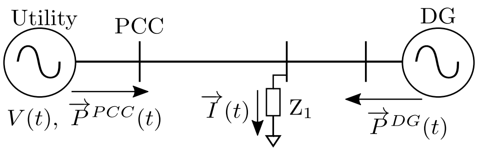

Figure 1. Equivalent model.

2.1. System Description

The utility power grid is assumed to be an infinite bar with ideal voltage regulation; therefore, it only provides positive sequence voltage at the fundamental frequency to the system. The continuous-time model of utility voltage is defined by (1). The current model, presented in (2), represents the total current demanded by the load. In these continuous-time equations, the subscript h denotes the h-th harmonic component, whereas supra-indices $\alpha\beta$ and $+-$ represent the real/complex and the symmetric components, respectively. For instance, $I_h^{\alpha+}$ denotes the real-positive sequence component of current harmonic h. Note that, according to (1) and (2), $\vec{V}$ and $\vec{I}$ represent vectors and V and I represent magnitudes.

$$\vec{V}(t) = \left[V_1^{\alpha+} + \jmath V_1^{\beta+}\right] = V_1\cos(\omega t) + \jmath V_1 \sin(\omega t) \qquad [V] \tag{1}$$

$$\begin{aligned} \vec{I}(t) &= \sum_{h=0}^{H}\left(\left[I_h^{\alpha+} + \jmath I_h^{\beta+}\right] + \left[I_h^{\alpha-} + \jmath I_h^{\beta-}\right]\right) \qquad [A] \\ \vec{I}(t) &= \sum_{h=0}^{H}\left(I_h^{+}[\cos(h\omega t + \phi_h) + \jmath\sin(h\omega t + \phi_h)] + I_h^{-}[\cos(h\omega t + \phi_h) - \jmath\sin(h\omega t + \phi_h)]\right) \ [A] \end{aligned} \tag{2}$$

By using (1) and (2), the real power delivered by the h-th current component is defined by (3).

$$\vec{P}_{Ih}(t) = V_1[I_h^{-}\cos((h+1)\omega t + \phi_h) + I_h^{+}\cos((h-1)\omega t + \phi_h)] \qquad [W] \tag{3}$$

Computing $P_{I(h-1)}$ and $P_{I(h+1)}$ (see (4)) and reorganizing the h-th power component, and the power balance necessary condition, are stated in (5) and (6), respectively.

$$\begin{aligned} P_{I(h-1)} &= V_1\left[I_{(h-1)}^{-}\cos(h\omega t + \phi_{h-1}) + I_{(h-1)}^{+}\cos((h-2)\omega t + \phi_{h-1})\right] \\ P_{I(h+1)} &= V_1\left[I_{(h+1)}^{-}\cos((h+2)\omega t + \phi_{h+1}) + I_{(h+1)}^{+}\cos(h\omega t + \phi_{h+1})\right] \end{aligned} \tag{4}$$

$$\vec{P}_h(t) = V_1[I_{h-1}^{-}\cos(h\omega t + \phi_{h-1}) + I_{h+1}^{+}\cos(h\omega t + \phi_{h+1})] \qquad [W] \tag{5}$$

$$\sum_{h=0}^{H} \vec{P}_h(t) = \sum_{h=1}^{H+1} \vec{P}_{I_h}(t) \tag{6}$$

Equation (6) is the truncated representation of the instantaneous real power balance for H harmonics components. In this case, the h = 0 component represents the active power referred to in the classical approach, whereas $h \neq 0$ components are excited according to the distortion disturbances. For instance, the $3h$ current components, which are excited by three-phase unbalanced loads, are related to $3h - 1$ and $3h + 1$ power harmonic components. Note that, according to (2) and (5), both I_{-1}^{-} and I_0^{+} do not have physical meaning, and, therefore, without loss of generality, can be assumed to be zero. Although it is not possible to state a one-to-one relation among current and power harmonics components, it is possible to state valid power-related inequalities to bound current components, as presented in the following subsection.

2.2. Power Bounds for Harmonics Current Mitigation

Computing the current vector magnitude, according to (2), Equation (7) is stated. Therefore, by using (3), the triangle Inequalities (8) and (9) are derived. Note that P_{Ih}^2 is at its maximum when positive and negative sequence current vectors match in the complex plane.

$$I_h^2 = \left[I_h^+ + I_h^-\right]^2 + \left[I_h^+ - I_h^-\right]^2 = 2\left(I_h^+\right)^2 + 2\left(I_h^-\right)^2 \tag{7}$$

$$\begin{aligned} I_h^2 &\geq \left[I_h^+ + I_h^-\right]^2 \quad [A^2] \\ I_h^2 &\geq \left[I_h^+ - I_h^-\right]^2 \quad [A^2] \end{aligned} \tag{8}$$

$$P_{Ih}^2 = \left|\vec{P}_{Ih}(t)\right|^2 \leq V_1^2\left[I_h^+ + I_h^-\right]^2 \leq V_1^2 I_h^2 \quad [W^2] \tag{9}$$

Computing $P_{I(h+1)}$ and $P_{I(h-1)}$ in (9):

$$P_{I(h+1)}^2 + P_{I(h-1)}^2 \leq V_1^2\left[I_{h+1}^+ + I_{h+1}^-\right]^2 + V_1^2\left[I_{h-1}^+ + I_{h-1}^-\right]^2 \tag{10}$$

By expanding (10) and defining $\mathbb{A} = 2I_{h+1}^+ I_{h+1}^- + (I_{h-1}^+)^2 + 2I_{h-1}^+ I_{h-1}^- + (I_{h+1}^-)^2 \quad [A^2]$, then $\mathbb{A} \geq 0$ and by using (5), inequality (11) is stated as follows.

$$\begin{aligned} P_{I(h+1)}^2 + P_{I(h-1)}^2 &\leq V_1^2\left[\left(I_{h-1}^-\right)^2 + \left(I_{h+1}^+\right)^2 + \mathbb{A}\right] \\ P_{I(h+1)}^2 + P_{I(h-1)}^2 &\leq P_h^2 + V_1^2\mathbb{A} \end{aligned} \tag{11}$$

Therefore, according to (9), Inequality (12) is valid to establish a set of H power components boundaries that satisfy $H + 1$ current requirements.

$$P_h^2 \leq V_1^2\left[I_{h+1}^2 + I_{h-1}^2\right] \; \forall \, 0 \leq h \leq H \tag{12}$$

In this sense, the current distortion requirements stated by IEEE std 1547, as a ratio of fundamental components, as well as the current Total Rated Distortion (TRD), can be interpreted as a set of inequalities in terms of adjacent power components. This set of inequalities allows the integration of power quality constraints in the MPC optimization problem.

3. Optimization Problem Formulation

MPC has shown remarkable results at the secondary control level and for power quality in microgrids; however, the considerable computational burden for its continuous-set implementation represents a barrier for managing harmonics compensation in power systems. In this regard, the Inequality (12) is valid because it is stated as a function of magnitudes of current and power harmonics components. Hence, using magnitude values for harmonics control opens the way for MPC implementations, as long as the phase angle required to inject each harmonic is computed locally without information about the power line impedance effect. To avoid ambiguity, supra-indices PCC and DG denote the source of power harmonics.

3.1. Synthesis of Model Constraints

Equalities and Inequalities (13) to (20) state the model constraints used to build the optimization problem, considering N steps ahead, since instant k. Since current controllers at the primary level should be tuned to respond against millisecond-order disturbances, it is possible to assume the steady state of these loops from the MPC point of view. Hence, the discrete-time incremental model, based on the forward Euler method, (13), are defined to predict power magnitudes of fundamental and harmonics frequencies. In this case, ΔU_h represents the change in the control action required to compensate for harmonics disturbances; therefore, an additional integrator should be placed at the controller output to compute U_h. Note that the integral action mitigates the steady state error; therefore $\Delta U_h = 0$ is hold, and, thus, the integrator output is the magnitude of the h-th harmonic component. The Inequality (14) is derived from Inequality (12), and bounds the harmonics injected by the compensator to the power grid. The upper bound, $P_{h,max}$, is constant along the whole prediction horizon and stated according to (15) and (16), where K_h is the ratio between I_1 and I_h. In addition, the slack variable $P_{h,s}$ is defined to avoid numerical infeasibilities by expanding, temporarily, the allowed range. Note that the lower bound of (14) is settled in zero because P_h^{PCC} refers to power component magnitudes.

$$\begin{aligned} P_0^{DG}(k{+}m) - P_0^{DG}(k{+}m{-}1) &= \Delta U_0(k{+}m{-}1) \qquad [W] \\ P_h^{PCC}(k{+}m) - P_h^{PCC}(k{+}m{-}1) &= \Delta U_h(k{+}m{-}1)\ \forall 1{\le}h{\le}H \qquad [W] \end{aligned} \tag{13}$$

$$0 \le P_h^{PCC}(k{+}m) \le P_{h,max} + P_{h,s}(k{+}m) \tag{14}$$

$$P_0^{PCC}(k) = I_1(k)V_1 \qquad [W] \tag{15}$$

$$P_{h,max} = \left(K_{h+1}^2 + K_{h-1}^2\right)^{\frac{1}{2}} P_0^{PCC}(k) \qquad [W] \tag{16}$$

The IEEE std 1547 [12] states the TRD, defined by (17), as a power quality index that relates the sum of all current harmonics, except the fundamental component I_1, with the rated current value, I_{rated}. However, when distributed generation is considered and I_{rated} changes, power quality requirements are relaxed. In this regard, a constraint related to the traditional current THD, that weights higher the variations of the fundamental current than the TRD [34], is preferred for control purposes. Therefore, the terminal THD Constraint (18) is defined as a function of the active power component, P_0^{pcc}, measured at instant k, and the predicted harmonic magnitudes P_h, at the end of the prediction horizon, both referred to the PCC, as shown (19). In the same way as (14), the slack variable THD_s is defined to avoid numerical infeasibilities by expanding, temporarily, the allowed range, and the lower bound of (18) is zero because THD is a function of power magnitudes.

$$TRD = \frac{\sqrt{I_{rms}^2 - I_1^2}}{I_{rated}} \times 100\% \tag{17}$$

$$0 \le THD(k{+}N) \le THD_{max} + THD_s(k{+}1) \tag{18}$$

$$THD(k{+}N) = \frac{\sum_{h=1}^{H} P_h^{PCC}(k{+}N)}{P_0^{PCC}(k)} \tag{19}$$

The last constraint considers the limitation due to the generation capacity of the DG. Inequality (20) computes the power balance through the prediction horizon, using, as the initial condition, the sum of power components delivered by the DG. This power balance considers the energy changes of each harmonic component ΔU_h. Considering that bidirectional power flows, caused by energy storage systems and interlinking converters in hybrid microgrids are not usual in mining facilities, the lower bound of power balance (20) is settled to zero.

$$0 \leq \sum_{h=0}^{H} P_h^{DG}(k) + \sum_{m=1}^{N}\sum_{h=0}^{H} \Delta U_h(k+m-1) \leq P_{cap} + P_{c,s}(k+1) \quad [W] \tag{20}$$

3.2. Cost Function Formulation

The cost Function (21) weighs, through the λ terms, the error of each power harmonic component delivered by the DG and its respective reference. For the fundamental component, P_0^{DG}, a regulation around the set point P_0^* is stated according to the generation capacity or the active power transferred between two microgrids when the DG is an interlinking converter. The other harmonic components are expected to be in the range defined by $P_{h,min}$ and $P_{h,max}$. To avoid possible infeasibility issues, the slack variable $P_{h,s}$ is strongly penalized, forcing the convergence of this control objective. In the same way, additional slack variables, $P_{c,s}$ and THD_s, are used in (18) and (20), to avoid infeasibility issues when power capacity and THD constraints are not numerically satisfied. The weighting terms were adjusted following the guidelines in [35], i.e., aiming for a trade-off between the control objectives and, if necessary, giving one objective a higher priority than the others. Other tuning methods, for instance, heuristic algorithms, such as particle swarm optimization (PSO) algorithm [36] or genetic algorithms [37], could be used. However, such methods require several tests and, in some cases, significant computational effort.

$$\begin{aligned} J = &\sum_{m=1}^{N}\sum_{h=0}^{H} \lambda_u \Delta U_h^2(k+m-1) + \sum_{m=1}^{N} \lambda_0 (P_0^*(k) - P_0^{DG}(k+m))^2 + \sum_{m=1}^{N}\sum_{h=1}^{H} \lambda_p P_{h,s}^2(k+m) \\ &+ \lambda_c P_{c,s}^2(k+1) + \lambda_T THD_s^2(k+1) \end{aligned} \tag{21}$$

The optimization problem, therefore, pursues the minimization of (21) subject to (13)–(16) and (18)–(20). This optimization problem is synthesized as a canonical quadratic programming (QP) problem, guaranteeing a global solution, being the optimized output vector composed of predicted values $\{P_0^{DG}(k+m), P_h^{PCC}(k+m), P_{h,s}(k+m), THD(k+N) \mid 1 \leq m \leq N, 1 \leq h \leq H\}$, and $\{\Delta U_h(k+m) \mid 1 \leq m \leq N, 0 \leq h \leq H\}$. From the MPC point of view, the values refer to the changes of the control action U_h required to achieve the active power reference P_0^* to the grid, and to control power harmonics $P_1^{PCC}, \ldots, P_H^{PCC}$. Note that in steady state $\Delta U_h = 0$ holds, the disturbances are mainly due to changes in the power harmonics profile on the load side. In the mining industry, the power consumption, and its harmonics profile, mainly depend on the features of the extracted materials [13], so the related disturbances cannot be forecast, amd only current measurements (see (15) and (16)), but not predictions, are included in the optimization problem.

The optimization is solved for every sampling period T_{MPC}, and only $\{\Delta U_h(k+1) \mid 0 \leq h \leq H\}$ are used in the rolling horizon scheme. Due to the computational burden of MPC increasing with the optimization vector length, the amount of harmonics to be compensated and the prediction horizon should be adjusted depending on the hardware platform where the MPC is deployed. On the other hand, convergence speed and damping are tuned according to the values of λ_u, λ_0, λ_p and λ_c. Details about MPC deployment are provided in the next section.

4. System Implementation and Results

As (5) states magnitude and phase angle for each harmonic component, if power measurements are decomposed, then, these components can be controlled independently.

In this sense, the proposed scheme for harmonics compensation uses a two-level hierarchy. The primary level is composed of a PI-based current control, where its reference is computed as a function of the local node voltage, and the power components, as shown in Figure 2.

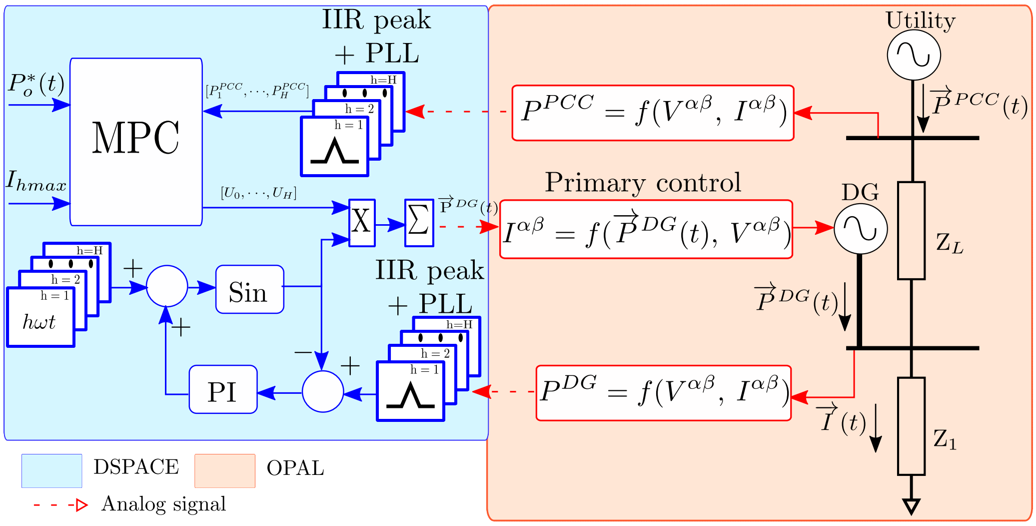

Figure 2. Proposed control diagram.

In order to preserve the proper synchronization, an additional PI control loop is required to adjust the phase angle, ϕ_h, according to the power decomposition estimated by a set of resonant Infinite Impulse Response (IIR-peak) filters. The resonant IIR-Peak type is a very-narrow bandpass filter, which is tuned to harmonic frequencies, preserving the magnitude inside the band, and mitigating frequencies outside it [38]. A PLL is used to estimate the instantaneous phase angle of each harmonic, which is compared locally with a phase oscillator. The whole primary control level and the three-phase three-wire power system of Figure 2 was deployed in an OPAL OP4510 real-time computer in a Hardware-In-the-Loop (HIL) configuration.

On the other hand, the secondary control level is composed of the proposed MPC, which is deployed in a MicroLabBox-dSPACE platform. The QP optimization problem is solved using OPTI-CasADi [39], and voltage and current measurements, used to compute real power, were acquired via analog inputs from the OPAL platform. The control actions represented by harmonics magnitudes were sent through analog outputs to the OPAL platform. Although MPC, based on QP problems for power quality improvement, has been reported, the proposed scheme integrates power-based constraints, instead of current or voltage constraints, extending the scope of the power quality issues to be addressed. For instance, the selective harmonics compensation technique, presented in [32], can be implemented by settling $P_{h,max}$ close to zero, whereas imbalance issues covered by [33] can be addressed by controlling triple harmonics. Another remarkable advantage of the proposed MPC is the IEEE std 1547 compliance, through harmonics management in a range, instead of a constant reference value. A detailed comparison is provided in Table 1, where the main features of the proposed scheme are compared against the approaches of [32,33]. Detailed information about the deployed algorithm used for MPC implementation is provided in Algorithm 1. Moreover, Figure 3 presents the HIL setup developed with the system parameters of Table 2.

Table 1. General Parameters.

Parameter	Description	Value
T_{MPC}	MPC Sampling Period	1 s
N	Prediction Horizon	5
V_1^{PCC}	PCC Voltage	1 P.U.
f_1	Fundamental Frequency	50 Hz
T_{IIR}	IIR-Peak filters Sampling Period	0.5 ms
T_{IIR}	IIR-Peak filters Bandwidth	5 Hz
T_{prim}	Primary level Sampling Period	0.2 ms
f_{prim}	Primary level natural frequency	1 kHz
Z_L	Line Impedance	0.68 + $\jmath$ 0.332 Ω

Algorithm 1 DMPC solution for harmonics compensation

Inputs: Measurements and estimations:
$\{[P_1^{PCC}(k), ..., P_H^{PCC}(k)]\} \rightarrow From\ IIR\ peak\ filters + PLLs$
Set points and optimization parameters:
$\{P_0^*(t), I_1(k), P_{cap}\}$
Outputs: $[U_0, ...U_H]$
Initialisation :
State $P_0^{PCC}(0) = P_0^*(0)$ and compute $P_{h,max}$ based on Equation (16).
for every k **do**
  Compute $P_0^{PCC}(k)$ and $P_{h,max}$ based on Equations (15) and (16).
  Update Inequality (18) based on (19).
  Update set point P_0^* in cost function (21).
  Solve QP problem using OPTI–CasADi framework.
  if Optimal solution is feasible and $t < k + T_{MPC}$ **then**
    Extract $[\Delta U_0(k+1), ...\Delta U_H(k+1)]$ from optimization output.
  else
    $[\Delta U_0(k+1), ...\Delta U_H(k+1)] = 0$.
  end if
  Send $[\Delta U_0(k+1), ...\Delta U_H(k+1)]$ to integrators to update controller outputs $[U_0(k+1), ..., U_H(k+1)]$
end for

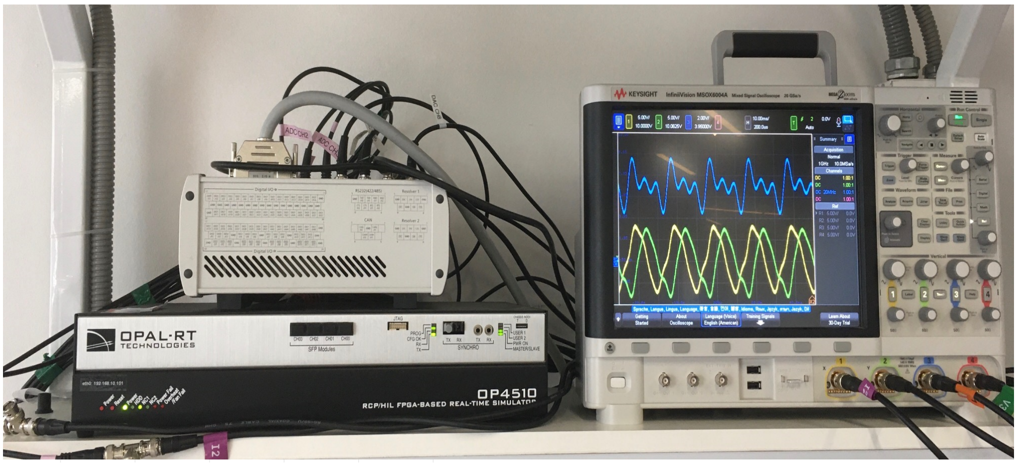

Figure 3. Real-time setup.

Table 2. Comparison against State-of-the-Art Techniques.

Parameter	Proposed	[32]	[33]
Continuous-set MPC	✓	✓	✓
Harmonics mitigation	✓	✓	×
Control level	Secondary	Primary	Secondary
Topology	Grid following	Grid following	Grid forming
Controlled Variable	Power	Current	Power and voltage
Optimized Power Quality Index	Harmonics and THD	Harmonics	Imbalances
Quadratic programming	✓	✓	✓
Reference Framework	$\alpha\beta$ magnitudes	*abc*	*abc*
Implementation	HIL	Simulation	HIL

Four cases were studied to provide evidence of the MPC capabilities related to selective harmonics mitigation, total current distortion, IEEE std 1547 compliance, and power capacity limitation. For all of these cases, the load was preserved as constant, demanding currents of 0.7 P.U. @ 50 Hz, 0.08 P.U. @ 100 Hz, and 0.05 P.U. @ 150 Hz and 200 Hz. A scale factor of 10× was used in analog inputs and outputs to visualize these signals properly. The system was started considering the DG disabled; therefore, the whole demand was supplied through the PCC, as shown Figure 4. The studied cases are presented in the following subsections.

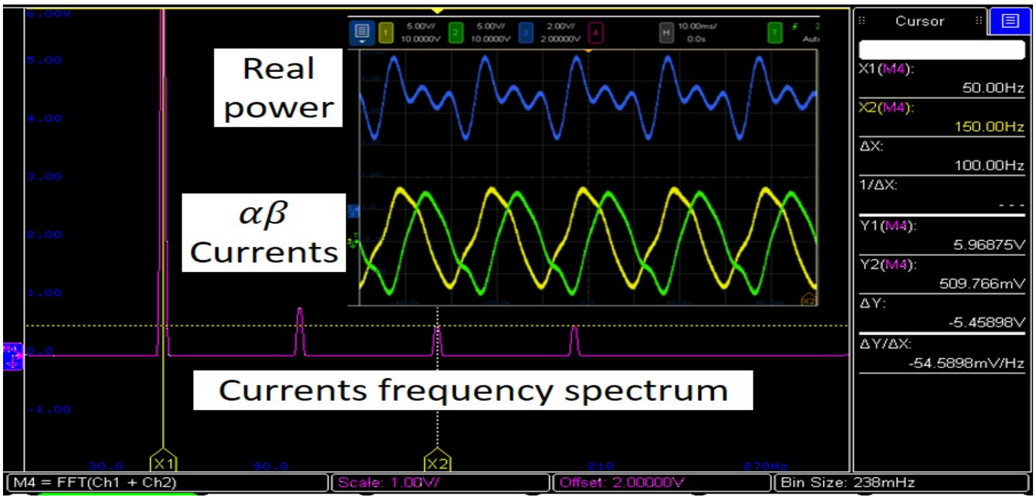

Figure 4. Power and $\alpha\beta$ currents delivered by the PCC without compensation.

4.1. Case 1: Compensation of Selected Harmonics

This scenario considered two periods as shown in Figure 5a. In the first period, the second and fourth current harmonics were compensated to zero references (Figure 5b); therefore, power supplied through the PCC was composed of a DC component and a 100 Hz component (Figure 5c). Note that, in Figure 4, the α and β currents had different DC values, which was corrected in Figure 5c. This was because, according to Inequality (12), by bounding P_1, current components I_0 and I_2 are controlled. However, this does not mean that unbalances are mitigated, as shown Figure 5c.

Figure 5. Power and currents delivered by the PCC and the DG for case 1: (**a**) PCC and DG power-Time domain. (**b**) Frequency spectrum and (**c**) time domain PCC signals when 3th harmonic was not compensated. (**d**) Frequency spectrum and (**e**) time domain signals when PCC was totally compensated.

The second period of case 1 considered the total compensation of harmonics in the PCC, as shown in Figure 5d,e. In this case, the power delivered through the PCC was close to a DC signal, which indicated that only active power was supplied from the utility to the load, whereas the DG supplied harmonic components. As shown in Figure 5a, an active power component (0.2 P.U.) was also supplied by the DG. Measured current values and the tuned weights of the MPC are shown in Table 3.

Table 3. Measured currents and weighting factors.

Period	I_1	I_2	I_3	I_4
0	7.1 100%	$\leq$0.8 11.42%	0.5 7.143%	$\leq$0.5 7.143%
	$P_0^{DG} = 0$		$THD^{PCC} = 25.7\%$	
1	4.65 100%	$\leq$0.01 0.2%	0.5117 11%	$\leq$0.01 0.02%
	$P_0^{DG} = 2$		$THD^{PCC} =$ 11.43%	
2	5.1 100%	$\leq$0.01 0.2%	0.0183 0.358%	$\leq$0.01 0.2%
	$P_0^{DG} = 2$		$THD^{PCC} = 0.75\%$	
$\lambda_u[1/W^2]$	$\lambda_0[1/W^2]$	$\lambda_p[1/W^2]$	$\lambda_c[1/W^2]$	λ_T
1	1	1e4	1e8	1e3

4.2. Case 2: Compensation of Total Current Distortion

In this case, λ_p was relaxed to provide evidence of the effect of the THD constraint. Similar to case 1, this test was divided into two periods, shown in Figure 6. The first period began when THD_{max} was settled to 5%, reducing the current harmonics, as shown in Figure 6a,b. Unlike case 1, none of the three current harmonics were totally mitigated, but current THD reduced from 25.7% to 2.45%; therefore, distortion on the PCC currents and power was allowed, as shown in Figure 6c.

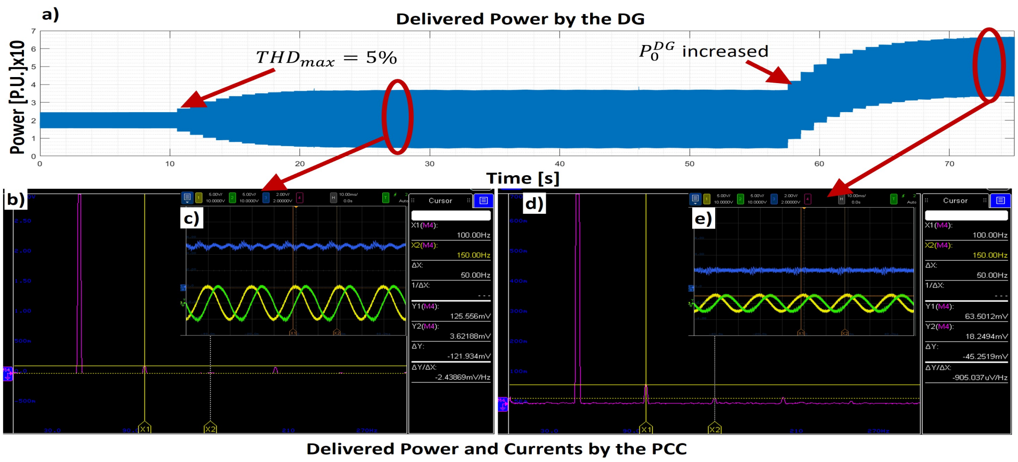

Figure 6. Power and currents delivered by the PCC and the DG for case 2: (**a**) DG power–time domain. (**b**) Frequency spectrum and (**c**) time domain PCC signals when THD_{max} was settled to 5%. (**d**) Frequency spectrum and (**e**) time domain signals when P_0^{DG} increased.

The second period began when the active power component supplied by the DG increased, but THD_{max} was preserved. In this case, distortion caused by harmonic components should also be reduced, because the PCC current at the fundamental frequency is reduced, preserving the power THD into the range stated by Inequality (18). Tuned weights and magnitudes of current harmonic components are shown in Table 4. According to the results, the current THD was lower than 5% in both periods; therefore, TRD requirements from IEEE std 1547 were satisfied as well.

Table 4. Measured currents and weighting factors.

Period	I_1	I_2	I_3	I_4
1	5.1 100%	0.125 2.45%	0.0036 0.07%	0.125 2.45%
	$P_0^{DG} = 2$		$THD^{PCC} =$ 4.972%	
2	2.5 100%	0.0635 2.54%	0.0183 0.732%	0.02 0.8%
	$P_0^{DG} = 5$		$THD^{PCC} =$ 4.072%	
$\lambda_u[1/W^2]$	$\lambda_0[1/W^2]$	$\lambda_p[1/W^2]$	$\lambda_c[1/W^2]$	λ_T
1	1	1	1e8	1e3

4.3. Case 3: IEEE std 1547 Current Distortion Compliance

For the third case, current harmonics boundaries and THD requirements were settled according to the IEEE std 1547. Due to $P_{h,max}$ values were not zero, and distortion on power signal was allowed, as shown in Figure 7a. In the same way, as shown Figure 7b, current components were in the range stated by (14) and (15). The highest being the the third harmonic, as it was allowed by the referred standard. Tuned weights, reference IEEE std 1547 values and measured currents are shown in Table 5.

Figure 7. Power and currents delivered by the PCC for case 3: (**a**) Time domain PCC signals and (**b**) Frequency spectrum when IEEE std 1547 compliance was settled.

Table 5. Measured currents and weighting factors.

Period	I_1	I_2	I_3	I_4
IEEE 1547	100%	1%	4%	2%
1	5.1 100%	0.48 0.941%	0.068 1.34%	0.035 0.687%
	$P_0^{DG} = 2$		THD^{PCC} = 2.968%	
$\lambda_u[1/W^2]$	$\lambda_0[1/W^2]$	$\lambda_p[1/W^2]$	$\lambda_c[1/W^2]$	λ_T
1	1	1e4	1e8	1e3

4.4. Case 4: Power Capacity Test

In this test, the DG was saturated, which meant that power requirements to satisfy harmonics compensation and active power delivery overran its power capacity. For this test, current I_1 was increased to 1 P.U. at the load to increase the current required for harmonics compensation, and settled to 5% at the beginning of period 1. As shown in Figure 8, the compensation requirements were satisfied, with the total power supplied by the DG being lower than its capacity. Around t = 100 s, P_0^* increased from 0.2 P.U. to 0.4 P.U. and, therefore, P_0^{DG} started its transition, but currents related to compensation were adjusted once $P_{h,max}$ was achieved, after 50 s, as shown Figure 9.

Since the new value of P_0^* was unachievable, the DG was saturated; however, harmonics compensation at the PCC was not altered. Finally, around t = 240 s, the set points $P_{h,max}$ were adjusted, according to IEEE std 1547. In this case, harmonics currents, as well as the fundamental component supplied by the DG, were rearranged at the end of period 2. The results associated to both aforementioned disturbances are shown in Figures 8b and 9. The current frequency spectrum and the time–domain signals of power and $\alpha\beta$ currents at the PCC are shown in Figure 8c,d. Note that, although current shapes were similar in both periods, power distortion at the beginning indicated more relaxed compensation requirements than the final state. Measured current values and parameters used in this test are shown in Table 6.

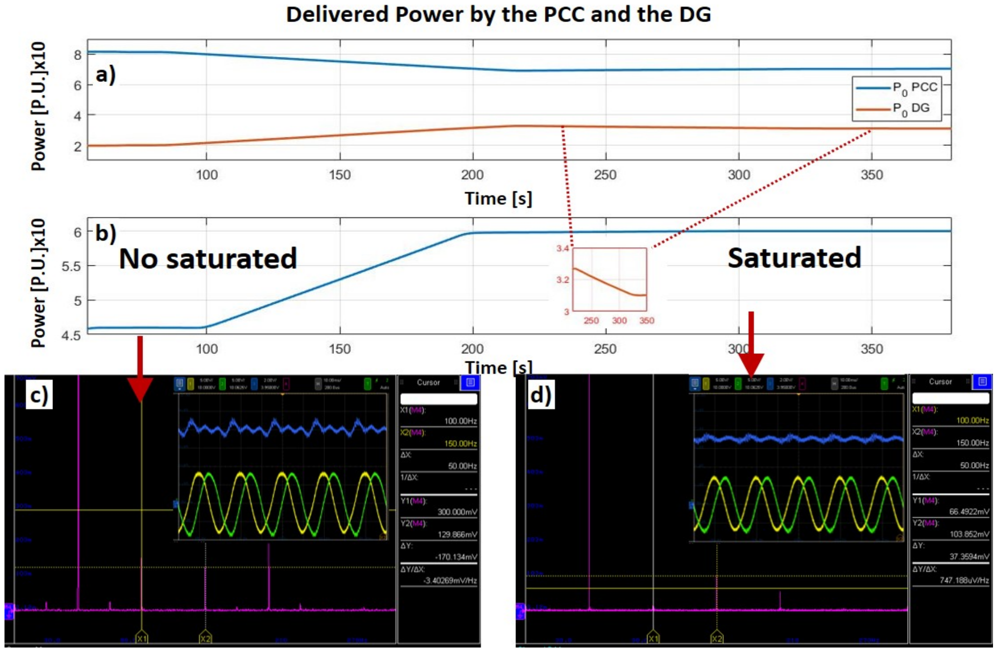

Figure 8. Power and currents delivered by the PCC and the DG for case 4: (**a**) time–domain PCC and DG active power signals, (**b**) total power supplied by the DG, (**c**) no saturated and (**d**) saturated measurements at the PCC.

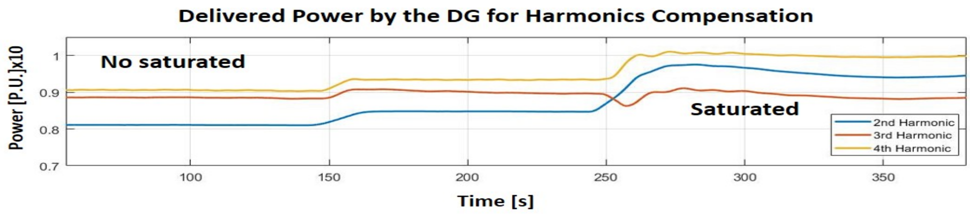

Figure 9. Power delivered by the DG for harmonics compensation.

Table 6. Measured currents and weighting factors.

Period	I_1	I_2	I_3	I_4
1	8 100%	0.3 3.75%	0.129 1.612%	0.2 2.5%
	$P_0^{DG} = 2$		$THD^{PCC} = 7.86\%$	
2	7 100%	0.0665 0.95%	0.103 1.471%	0.06 0.857%
	$P_0^{DG} = 3$		$THD^{PCC} = 3.278\%$	
$\lambda_u[1/W^2]$	$\lambda_0[1/W^2]$	$\lambda_p[1/W^2]$	$\lambda_c[1/W^2]$	λ_T
1	1	1e4	1e8	1e3

4.5. Analysis

Four different cases were presented to evidence the proposed MPC capabilities related to low-frequency harmonics compensation. Although the computational burden of MPC applications is recognized, the proposed scheme allows the integration of power quality constraints referred to the IEEE std 1547.

Cases 1 and 2 showed the capabilities of the proposed scheme, i.e., selective harmonics and THD compensation, respectively. Each one of these cases demonstrated that the system currents were, individually, in the expected range, due to the power Constraints (14) (case 1) and (18) (case 2). The controller was able to properly compensate for harmonics and current distortion. In the same way, case 3 presents the results when both aforementioned constraints were settled according to the IEEE std 1547. In this case, the second current harmonic was close to its maximum value, but the third and the fourth harmonics were lower to preserve $THD^{PCC} \leq 5\%$, as the standard requires.

Similarly, case 4 showed the system performance when the DG was saturated. In this case, the saturation was due to an over-rated active power reference. The results showed that power quality objectives were prioritized over active power transference. This is because active power used for mining activities is mainly supplied by third-party power purchase agreements; therefore, generation is not the main topic in the mining industry. In contrast, promoting high power quality requirements in mining power systems reduces not only operational expenditures but also power system failures.

The four cases analyzed demonstrated that the proposed MPC scheme is able to compensate for harmonics and current distortion effects without adding additional power converters. Instead, these capabilities are embedded in the control system of the DGs. This is of great importance, as implementation costs are reduced and no hardware intervention is needed. Moreover, the MPC strategy fulfils the requirements of the IEEE 1547 standard, while the maximum power ratings of the DGs are respected. The proposed MPC strategy presents a better solution than PI-based approaches, as with these approaches it is hard to include constraints in the controlled variables and to achieve multiple objectives at the same time. Finally, note that the four cases analyzed were validated via hardware-in-the-loop experiments.

5. Conclusions and Final Remarks

In this paper, a novel MPC strategy for power quality improvement was presented. The proposed scheme is deployable in mining industry environments once power systems of mining facilities are affected by low order harmonics (below 200 Hz), which are not easily filtered, even when AFE converters are used as the interface between rotary machines and the power grid. In this sense, the proposed controller optimizes the power required for harmonics compensation and prioritizes this objective over active power delivery to preserve the power quality inside the power system. Furthermore, the proposed optimization can be executed for real-time applications, once formulated in terms of harmonics magnitudes, allowing more extended sampling periods than the primary control level continuous-set implementations and integrating more restrictive constraints than reported in the reviewed literature.

Although the results shown in this paper are promising, compensating harmonics pollution only in the PCC of mining facilities is not the most efficient scheme because harmonics currents are circulating through the power system. In this sense, some assumptions that our proposed scheme relies on should be covered by future research. The most important assumption is related to the a priori knowledge of harmonics components to be compensated, considering that, in mining facilities, harmonics profiles depend on machinery speed. In this sense, the deployment of computationally efficient methods of harmonics components provides additional features; therefore, the proposed control can be extended to consider this feature. Another open challenge relates to the development of distributed algorithms that allow cooperative compensation for multi-node power grids, which is the case for mining facilities. In this case, the challenge is to find an optimal information management system to reduce the performance requirements on the communication network (bandwidth, latency, and channel capacity), without sacrificing control performance.

Author Contributions: Conceptualization, J.S.G. and L.T.; methodology, L.T.; software, J.S.G.; validation, A.N.-F. and C.G.; formal analysis, J.S.G., L.T. and F.N.; investigation, A.N.-F.; resources, F.F.-B.; data curation, A.N.-F.; writing—original draft preparation, J.S.G. and A.N.-F.; writing—review and editing, L.T., A.Z.C. and F.F.-B.; visualization, A.N.-F.; supervision, F.N., J.R. and A.Z.C.; project administration, F.N.; funding acquisition, F.N. All authors have read and agreed to the published version of the manuscript.

Funding: This work was partially funded by ANID under grant ANID PIA ACT192013. F.F.-B. acknowledge the support of SERC Chile (CONICYT/FONDAP/15110019). C.G. and J.R. acknowledge the support of ANID/FONDECYT through projects FB0008, 1210208 and 1221293.

Institutional Review Board Statement: Not applicable.

Informed Consent Statement: Not applicable.

Data Availability Statement: Not applicable.

Conflicts of Interest: The authors declare no conflict of interest.

Abbreviations

The following abbreviations are used in this manuscript:

AFE	Active front end
PCC	Point of common coupling
MPC	Model predictive control
DG	Distributed Generator
TRD	Total Rated Distortion
THD	Total Harmonic Distortion
PLL	Phase locked loop
PWM	Pulse width modulation
QP	Quadratic Programming

References

1. Moreno-Leiva, S.; Haas, J.; Junne, T.; Valencia, F.; Godin, H.; Kracht, W.; Nowak, W.; Eltrop, L. Renewable energy in copper production: A review on systems design and methodological approaches. *J. Clean. Prod.* **2020**, *246*, 118978. [CrossRef]
2. Haas, J.; Moreno-Leiva, S.; Junne, T.; Chen, P.J.; Pamparana, G.; Nowak, W.; Kracht, W.; Ortiz, J.M. Copper mining: 100% solar electricity by 2030? *Appl. Energy* **2020**, *262*, 114506. [CrossRef]
3. Symonds, A.; Laylabadi, M. Cycloconverter Drives in Mining Applications: A Typical Industrial System Is Analyzed and the Impact of Harmonic Filtering Considered. *IEEE Ind. Appl. Mag.* **2015**, *21*, 36–46. [CrossRef]
4. Siemens. *Drives for Every Demand Core Applications and Product Highlights Digitalization Offering*; Siemens AG: Nuremberg, Germany, 2019.
5. Parreiras, T.M.; Justino, J.C.G.; Rocha, A.V.; de Jesus Cardoso Filho, B. True Unit Power Factor Active Front End for High-Capacity Belt-Conveyor Systems. *IEEE Trans. Ind. Appl.* **2016**, *52*, 2737–2746. [CrossRef]
6. Schutzhold, J.; Benath, K.; Muller, V.; Hofmann, W. Design criteria for energy efficient belt conveyor drives. In Proceedings of the 2014 International Symposium on Power Electronics, Electrical Drives, Automation and Motion, Ischia, Italy, 18–20 June 2014; pp. 1256–1263.
7. Cruzat, J.V.; Valenzuela, M.A. Modeling and Evaluation of Benefits of Trolley Assist System for Mining Trucks. *IEEE Trans. Ind. Appl.* **2018**, *54*, 3971–3981. [CrossRef]
8. Siemens Mobile Mining Industry. *SIMINE Haul Truck*; Siemens AG: Nuremberg, Germany, 2019.
9. Aravena, P.A.; Moran, L.A.; Burgos, R.; Astudillo, P.; Olivares, C.; Melo, D.A. High-Power Cycloconverter for Mining Applications: Practical Recommendations for Operation, Protection, and Compensation. *IEEE Trans. Ind. Appl.* **2015**, *51*, 82–91. [CrossRef]
10. Moran, L.; Albistur, C.A.; Burgos, R. Multimega VAR Passive Filters for Mining Applications: Practical Limitations and Technical Considerations. *IEEE Trans. Ind. Appl.* **2016**, *52*, 5310–5317. [CrossRef]
11. Yaghoobi, J.; Abdullah, A.; Kumar, D.; Zare, F.; Soltani, H. Power Quality Issues of Distorted and Weak Distribution Networks in Mining Industry: A Review. *IEEE Access* **2019**, *7*, 162500–162518. [CrossRef]
12. *IEEE Std. 1547-2018*; Standard for Interconnection and Interoperability of Distributed Energy Resources with Associated Electric Power Systems Interfaces. IEEE: New York, NY, USA, 2018; pp. 1–138.
13. Gomez, J.S.; Rodriguez, J.; Garcia, C.; Tarisciotti, L.; Flores-Bahamonde, F.; Pereda, J.; Nunez, F.; Cipriano, A.Z.; Salas, J.C. An Overview of Microgrids Challenges in the Mining Industry. *IEEE Access* **2020**, *8*, 191378–191393. [CrossRef]
14. Mirzaeva, G.; Carter, D.; Uddin, M.; Stepien, P. Electrically safe variable speed drive for underground mining applications. In Proceedings of the 2019 IEEE Industry Applications Society Annual Meeting, Baltimore, MD, USA, 29 September–2 October 2019; pp. 1–8.
15. Hosseinzadeh, M.; Salmasi, F.R. Robust Optimal Power Management System for a Hybrid AC/DC Micro-Grid. *IEEE Trans. Sustain. Energy* **2015**, *6*, 675–687. [CrossRef]
16. Yang, D.; Zhou, Z.; Liu, Y.; Jiang, J. Modeling of Dual-PWM Adjustable Speed Drives for Characterizing Input Interharmonics Due to Torque Oscillations. *IEEE J. Emerg. Sel. Top. Power Electron.* **2021**, *9*, 1565–1577. [CrossRef]
17. Zhao, Z.; Zhang, J.; Yan, B.; Cheng, R.; Lai, C.S.; Huang, L.; Guan, Q.; Lai, L.L. Decentralized Finite Control Set Model Predictive Control Strategy of Microgrids for Unbalanced and Harmonic Power Management. *IEEE Access* **2020**, *8*, 202298–202311. [CrossRef]

18. Yao, J.; Zhu, W.; Meng, L.; Lin, H.; Shu, Z.; Liu, L. Unbalanced Harmonic Suppression of Three-Level Active Power Filter with Optimal Hybrid Control. In Proceedings of the 2019 IEEE 10th International Symposium on Power Electronics for Distributed Generation Systems (PEDG), Xi'an, China, 3–6 June 2019; pp. 207–211.
19. Liu, C.; Xing, X.; Du, C.; Zhang, B.; Zhang, C.; Blaabjerg, F. An Improved Model Predictive Control Method Using Optimized Voltage Vectors for Vienna Rectifier With Fixed Switching Frequency. *IEEE Trans. Power Electron.* **2023**, *38*, 358–371. [CrossRef]
20. Liu, T.; Chen, A.; Huang, Y. Multi-Vector Model Predictive Current Control for Paralleled Three-Level T-Type Inverters With Circulating Current Elimination. *IEEE Trans. Ind. Electron.* **2022**, 1–11. [CrossRef]
21. Akagi, H.; Watanabe, E.H.; Aredes, M. *Instantaneous Power Theory and Applications to Power Conditioning*; John Wiley & Sons, Inc.: New York, NY, USA, 2006; pp. 1–379.
22. Tenti, P.; Paredes, H.K.M.; Mattavelli, P. Conservative Power Theory, a Framework to Approach Control and Accountability Issues in Smart Microgrids. *IEEE Trans. Power Electron.* **2011**, *26*, 664–673. [CrossRef]
23. Gomez, J.S.; Llanos, J.; Espina, E.; Burgos-Mellado, C.; Rodriguez, J. Cooperative Power Conditioners for Microgrids in Mining. In Proceedings of the 2021 23rd European Conference on Power Electronics and Applications (EPE'21 ECCE Europe), Ghent, Belgium, 6–10 September 2021; pp. P.1–P.10.
24. Morales-Paredes, H.K.; Burgos-Mellado, C.; Bonaldo, J.P.; Rodrigues, D.T.; Quintero, J.S.G. Cooperative Control of Power Quality Compensators in Microgrids. In Proceedings of the 2021 IEEE Green Technologies Conference (GreenTech), Denver, CO, USA, 7–9 April 2021; pp. 380–386.
25. He, J.; Li, Y.W.; Munir, M.S. A Flexible Harmonic Control Approach Through Voltage-Controlled DG–Grid Interfacing Converters. *IEEE Trans. Ind. Electron.* **2012**, *59*, 444–455. [CrossRef]
26. Wodyk, S.; Iwanski, G. Active power filter control with vibrating coordinates transformation. *IEEE Trans. Power Deliv.* **2022**, *38*, 1–12. [CrossRef]
27. Burgos-Mellado, C.; Llanos, J.; Espina, E.; Sáez, D.; Cárdenas, R.; Sumner, M.; Watson, A. Single-Phase Consensus-Based Control for Regulating Voltage and Sharing Unbalanced Currents in 3-Wire Isolated AC Microgrids. *IEEE Access* **2020**, *8*, 164882–164898. [CrossRef]
28. Burgos-Mellado, C.; Llanos, J.J.; Cárdenas, R.; Sáez, D.; Olivares, D.E.; Sumner, M.; Costabeber, A. Distributed Control Strategy Based on a Consensus Algorithm and on the Conservative Power Theory for Imbalance and Harmonic Sharing in 4-Wire Microgrids. *IEEE Trans. Smart Grid* **2020**, *11*, 1604–1619. [CrossRef]
29. Zhou, X.; Tang, F.; Loh, P.C.; Jin, X.; Cao, W. Four-leg converters with improved common current sharing and selective voltage-quality enhancement for islanded microgrids. *IEEE Trans. Power Deliv.* **2016**, *31*, 522–531. [CrossRef]
30. Meng, L.; Zhao, X.; Tang, F.; Savaghebi, M.; Dragicevic, T.; Vásquez, J.C.; Guerrero, J.M. Distributed voltage unbalance compensation in islanded microgrids by using a dynamic consensus algorithm. *IEEE Trans. Power Electron.* **2016**, *31*, 827–838. [CrossRef]
31. Zhou, J.; Kim, S.; Zhang, H.; Sun, Q.; Han, R. Consensus-based distributed control for accurate reactive, harmonic, and imbalance power sharing in microgrids. *IEEE Trans. Smart Grid* **2018**, *9*, 2453–2467. [CrossRef]
32. Skjong, E.; Suul, J.A.; Rygg, A.; Johansen, T.A.; Molinas, M. System-Wide Harmonic Mitigation in a Diesel-Electric Ship by Model Predictive Control. *IEEE Trans. Ind. Electron.* **2016**, *63*, 4008–4019. [CrossRef]
33. Navas-Fonseca, A.; Burgos-Mellado, C.; Gomez, J.S.; Donoso, F.; Tarisciotti, L.; Saez, D.; Cardenas, R.; Sumner, M. Distributed Predictive Secondary Control for Imbalance Sharing in AC Microgrids. *IEEE Trans. Smart Grid* **2022**, *13*, 20–37. [CrossRef]
34. Arranz-Gimon, A.; Zorita-Lamadrid, A.; Morinigo-Sotelo, D.; Duque-Perez, O. A Review of Total Harmonic Distortion Factors for the Measurement of Harmonic and Interharmonic Pollution in Modern Power Systems. *Energies* **2021**, *14*, 6467. [CrossRef]
35. Rossiter, J. *Model-Based Predictive Control: A Practical Approach (Control Series)*, 1st ed.; CRC Press: Boca Raton, FL, USA, 2017.
36. Suzuki, R.; Kawai, F.; Ito, H.; Nakazawa, C.; Fukuyama, Y.; Aiyoshi, E. Automatic Tuning of Model Predictive Control Using Particle Swarm Optimization. In Proceedings of the 2007 IEEE Swarm Intelligence Symposium, Honolulu, HI, USA, 1–5 April 2007; pp. 221–226.
37. Van der Lee, J.; Svrcek, W.; Young, B. A tuning algorithm for model predictive controllers based on genetic algorithms and fuzzy decision making. *ISA Trans.* **2008**, *47*, 53–59. [CrossRef]
38. Orfanidis, S.J. *Introduction to Signal Processing*; Prentice-Hall, Inc.: Cliffs, NJ, USA, 1995.
39. Andersson, J.A.E.; Gillis, J.; Horn, G.; Rawlings, J.B.; Diehl, M. CasADi: A software framework for nonlinear optimization and optimal control. *Math. Program. Comput.* **2019**, *11*, 1–36. [CrossRef]